CW difference frequency generation using $AgGaS_2$: problems encountered in power scaling

Charles E. Miller, Wade C. Eckhoff, Ulrich Simon, Frank K. Tittel, and Robert F. Curl

Department of Chemistry and Rice Quantum Institute
PO Box 1892, Rice University, Houston, TX 77251-1892
e-mail: CEMILLE@ricevm1.rice.edu

ABSTRACT

We report the results of our efforts to increase the infrared output power from a cw difference frequency generation source based on the non-linear material $AgGaS_2$ for use in infrared kinetic spectroscopy. Experimental and theoretical infrared conversion efficiencies are compared as a function of pump power, signal power, and focusing conditions. The predicted and observed IR yields agree well for the unfocused beam; however, the agreement is poor (experimental conversion a factor of 3-5 less than theory) for all focused conditions. The highest IR output powers obtained corresponded to experimental conditions which are slightly over-focused compared to the theoretical optimum. Thermal loading of the $AgGaS_2$ decreases the parametric conversion efficiency when the power in one of the input lasers beams exceeds ~800 mW. Infrared powers of 10 - 30 μW have been achieved near 5.2 μm. Future improved crystals should yield powers at the ~500 μW level.

1. INTRODUCTION

We are developing cw difference frequency generation (DFG) in $AgGaS_2$ as a probe source for infrared kinetic spectroscopy (IRKS). Before addressing the technical aspects of DFG in $AgGaS_2$, it seems appropriate to discuss the end use. IRKS has proven to be a powerful tool for studying the spectroscopy of free radicals and for following their chemical kinetics.[1-4] The real power of this technique lies in its ability to distinguish between different absorbing species by frequency and/or temporal discrimination with nearly universal detection, as the vast majority of molecules have at least one infrared active vibration in the 2 - 20 μm fingerprint region. The IRKS technique is reasonably sensitive, allowing detection of number densities as low as 10^{12} molecules cm^{-3}.

The performance characteristics of this IR probe almost exclusively determine the feasibility of any experiments we desire to conduct: thus the crucial element of any IRKS experimental apparatus is the infrared source. The ideal IRKS probe source meets a demanding set of performance criteria. It is continuously tunable over the entire 2 - 20 μm IR fingerprint region. A spectral bandwidth of at most a few MHz is required for high resolution spectroscopy. A cw source is desirable so that the complete temporal profile of the interrogated species may be obtained during each experimental duty cycle. The source must provide infrared power levels adequate to perform the desired experiments. We have constructed a cw difference frequency generation source based on the nonlinear material $AgGaS_2$ which completely covers the 3 - 10 μm portion of the fingerprint region and has a bandwidth of ~1 MHz. This paper presents our successful efforts to achieve the "adequate infrared power levels" necessary for IRKS experiments.

2. THEORY

Several groups[5-7] have derived the expression for the IR power created by the three wave parametric interaction encountered in the difference frequency mixing of focused gaussian beams

$$P_i = \frac{P_p P_s (2 \omega_i d_{eff})^2}{n_p n_s n_i c^3 \pi \varepsilon_0} \frac{h(\mu,\xi) L}{(|k_p|^{-1} + |k_s|^{-1})} \qquad (1)$$

0-8194-1440-9/94/$6.00

Here the subscripts p, s, and i refer to the pump, signal, and idler waves, respectively, and the convention $\omega_p > \omega_s > \omega_i$ has been followed; P is the appropriate laser power; d_{eff} is the effective nonlinear coefficient and $d_{eff} = 12$ pm V^{-1} for $AgGaS_2$ [8]; L is the crystal length, 45 mm for our crystal; k is the appropriate wave vector; the dimensionless parameters μ and ξ are the ratio of the input wave vector magnitudes ($\mu = |k_s|/|k_p|$) and the ratio of the crystal length to the confocal parameter of the input beams ($\xi = L/b$); the function $h(\mu,\xi)$ reflects the focusing conditions. Equation (1) is in the form appropriate to the definition of d_{eff} normally used for mks units.

In the limit of no focusing $\xi \rightarrow 0$ and $h(\mu,\xi) \rightarrow \xi$ and Equation (1) can be reduced to the more widely recognized plane wave limit

$$P_i = \frac{P_p P_s (2 \omega_i d_{eff})^2}{n_p n_s n_i c^3 \pi \varepsilon_0} \frac{L^2}{(w_p^2 + w_s^2)} \qquad (2)$$

where w_p and w_s are the radii for the pump and signal waves in the crystal. The principal difference between Equations (1) and (2) is that the $h(\mu,\xi)$ function drops out of Equation (2) and there is a quadratic dependence of the infrared power on the crystal length in the plane wave limit. Both expressions vary linearly in P_p and P_s and quadratically in ω_i and d_{eff}.

The function $h(\mu,\xi)$ contains all of the focusing information for the DFG process and is given by

$$h(\mu,\xi) = \frac{1}{2\xi} \int_0^{\xi} d\tau'' \int_{-\xi}^{\xi} d\tau' \frac{1 + \tau'\tau''}{(1+\tau'\tau'')^2 + (\tau' - \tau'')^2 \left[\frac{1+\mu^2}{1-\mu^2}\right]^2} \qquad (3)$$

There is no analytic expression for this integral. Figure 1 illustrates the variation of $h(\mu,\xi)$ with ξ for several fixed values of μ. For a given set of P_p and P_s, it is obvious that to maximize P_i one should maximize $h(\mu,\xi)$. As shown in Figure 1, the maximum of the $h(\mu,\xi)$ function is quite peaked for smaller μ values, but as $\mu \rightarrow 1$ the function is very flat in the vicinity of the maximum and variations in ξ do not significantly alter $h(\mu,\xi)$.

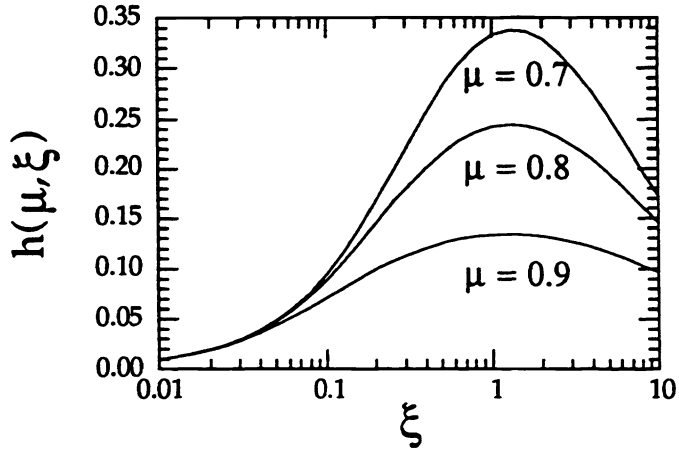

Figure 1.
The function $h(\mu,\xi)$.

3. EXPERIMENTAL RESULTS

The experimental apparatus used in the power measurement experiments has been described in detail previously.[1] Two Coherent 899 single mode ring lasers provide the pump and signal beams. The polarization of the pump laser is rotated 90° to achieve proper phase matching orientation, and the two beams are spatially overlapped using a polarization beamsplitter cube in reverse. The copropagating beams are then focused into the middle of a 45 mm long $AgGaS_2$ crystal (Cleveland Crystals Inc.) to produce

infrared radiation. The IR output is collimated and then focused onto the active element of a 1 mm diameter InSb detector (Infrared Associates). The visible beams are rejected prior to the detector by placing a AR coated Ge flat in the beam path. Modulated IR signals are observed using lock-in amplifier (PAR) and an oscilloscope (Phillips). A value of 2500 mV/μW for the detector/preamplifier combination [based on a detector responsivity of 2.5 A/W, a preamp transimpedance of 10^5 V/A, and secondary voltage amplification of 10] was used to convert all experimental voltage measurements into IR powers.

The $AgGaS_2$ crystal used in these experiments was fabricated in 1991 by Cleveland Crystal and cut for 90° type I phase matching. Both front and rear faces are polished to λ/8 flatness (relative to 632.8 nm) and there is a 1° wedge in the exit surface to prevent accidental etaloning. The nominal transparency range of this material extends from the electronic band gap transition near 500 nm to the phonon absorption edge at 10 μm.[9,10] Absorption coefficients of 4.2% cm^{-1} at 632.8 nm and 1.6% cm^{-1} at 1064 nm were determined for this crystal by the manufacturer using calorimetric methods. Figure 2 compares the transmission characteristics of the crystal between 630 and 840 nm measured using the ring lasers to the transmission efficiency calculated for a crystal having only Fresnel losses at the entrance and exit surfaces. The observed values and wavelength dependence of the transmission efficiency are in reasonably good agreement with those predicted by the calorimetry measurements, although it is difficult to accurately measure absolute values for the absorption coefficient due to the large index of refraction for $AgGaS_2$. This crystal was used without anti-reflection (AR) coatings since the AR coatings on previous $AgGaS_2$ pieces had been burned into the surfaces by the visible lasers.

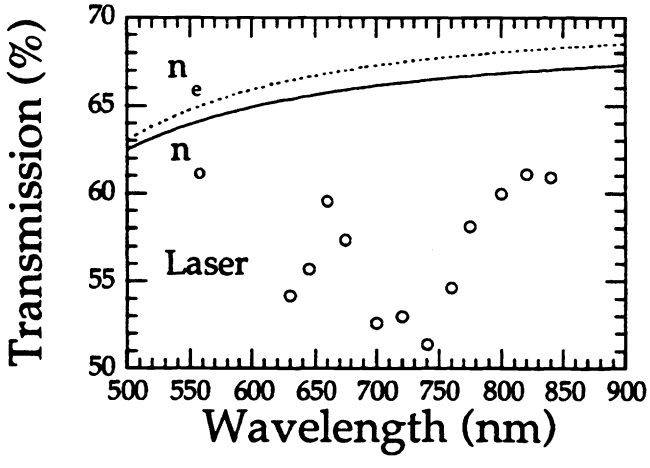

Figure 2. The transmission spectrum of the 45 mm $AgGaS_2$ crystal. The open circles (O) were measured using the 899 ring lasers. The calculated transmission from Fresnel reflection losses for n_e and n_o are given for reference.

The IR power measurements were performed at 1903.3 cm^{-1}, the peak of the InSb detector spectral response function. The pump and signal waves required to produce IR at this frequency are ν_p = 15013.3 cm^{-1} (666.076 nm) and ν_s = 13,110.0 cm^{-1} (762.776 nm). The corresponding value for μ is 0.8775. The values of $h(\mu=0.8775,\xi)$ are approximately shown for the μ = 0.9 curve in Figure 1. The value $h_{max}(\mu=0.8775,\xi)$ occurs for ξ~1.125 and the function displays minimal dependence on the focusing parameter for ξ ~ 0.7 to 2.2.

IR powers were measured for a series of focusing conditions (focal lengths F = ∞, 400 mm, 250 mm, and 100 mm) by placing a lens in the path of the copropagating beams such that the calculated position of the beam waist was at the center of the $AgGaS_2$ crystal. The pump laser power (P_p) was fixed by introducing neutral density filters into its path and measuring the power just prior to the $AgGaS_2$ crystal. The signal laser power (P_s) was subsequently varied, also using neutral density filters, and the resulting IR power recorded as a function of F, P_p, and P_s. Results for the case of F = ∞ (no focusing lens or the plane wave approximation) and F = 100 mm are shown in Figures 3 and 4.

The experimentally observed IR powers increased with tighter focusing for all of the lenses employed in this study. Table I lists the experimental and theoretical IR powers for all of the focusing conditions used in this study. For μ = 0.8775, the maximum IR power yield predicted by Equation (1) occurs for ξ = 1.125. Using our experimental configuration, this would require a lens having F ~ 165 mm. It is apparent from the experimental results that slight over focusing provides increased IR power compared

to the calculated optimum, although $h(\mu,\xi)$ for the most tightly focused case considered (F = 100 mm, ξ = 1.893) only differs by 1% from the maximum possible value.

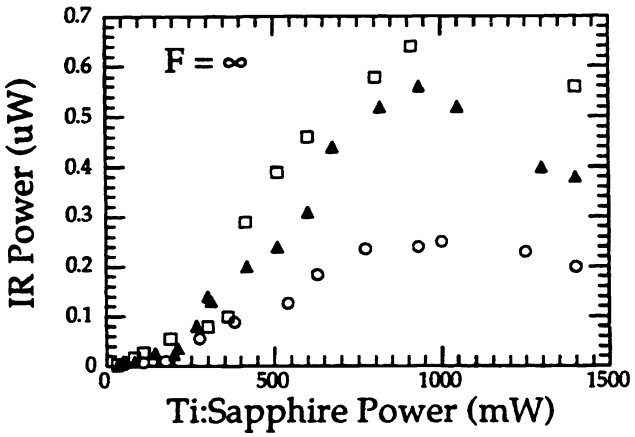

Figure 3. IR power generated as a function of the signal laser power for the case of no focusing. The three fixed pump laser powers are 50 mW (O), 100 mW (▲), and 200 mW(□).

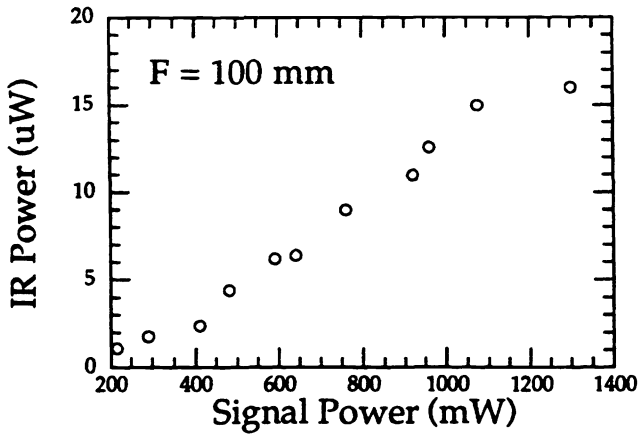

Figure 4. IR power generated as a function of the signal laser power for the case of F = 100 mm. The pump laser power was fixed at 110 mW.

TABLE I. Experimental and Calculated IR Powers.

F (mm)	ξ	$h(\mu,\xi)$	[a]Calc. P_i ($\mu W/W^2$)	[b]Expt. P_i ($\mu W/W^2$)	Expt./Calc.
∞	0.003	0.003	7.1	5.5	0.775
400	0.063	0.056	101	22	0.218
250	0.224	0.118	215	42.7	0.198
100	1.893	0.159	288	109	0.378

a. Calculated powers have been corrected for Fresnel losses at the entrance and exit surfaces of the crystal.

b. Experimental IR power efficiencies were determined from the linear portion of the P_i vs. P_S curve, as described in the text.

The curves in Figures 3 and 4 illustrate the typical characteristics observed when attempting to maximize the IR power output. For a fixed value of P_p, there are three distinct IR conversion regimes as a function of P_S. For $P_S \leq 200$ mW the IR power scales linearly with P_S, but the slope efficiency is less than that observed for the intermediate power regime. This is most likely due to the choice of phase matching frequencies which are optimized for higher input powers. For intermediate input power levels, 200 mW $\leq P_S \leq$ 800 mW, the IR power output is still a linear function of P_S, but the conversion efficiency is improved. For $P_S \geq 800$ mW there is a marked decrease in the IR power output. This decrease in power is usually accompanied by a noticeable "blooming" of the visible beams that have passed through the crystal. At higher input powers we also observe a slow, time dependent shift in the frequency associated with the maximum IR power output.

4. ANALYSIS

The single mode ring lasers used in this work have excellent gaussian beam properties, although there may be some slight astigmatism when the laser cavities are optimized for maximum TEM_{00} output power.[11] Measured values of M^2 for the lasers used in this study were 1.0 within the 5% experimental uncertainty of the measuring process. Therefore, purely gaussian beam behavior was assumed in the analysis. The pump and signal beam parameters were calculated assuming that ω_0(pump) = 275 μm, $\theta_{1/2}$(pump) = 0.80 mrad, ω_0(signal) = 285 μm, $\theta_{1/2}$(pump) = 0.85 mrad and that the ω_0 position for each laser was located at the output coupler. The desired beam properties at any point along the propagation path were then obtained by computing the appropriate ABCD matrix algebra. Of special interest are the confocal parameters

$$b_p = \frac{2\pi n_e(\lambda_p)\,\omega_p^2}{\lambda_p} \qquad b_S = \frac{2\pi n_o(\lambda_S)\,\omega_S^2}{\lambda_S} \qquad (4a, 4b)$$

since these values determine ξ. We note that b is defined in the non-linear medium and must necessarily include the index of refraction factor. The propagation distances were adjusted so that the calculated ξ values for the pump and signal beams were approximately equal and a single value was used for both beams in subsequent power calculations.

The agreement between theory and experiment is quite good for the case of unfocused beams (Table I). The experimental P_i yield is 77.8% of the predicted IR power and there is very good consistency between the determinations made for different values of the pump laser power. The calculated power levels obtained from Equations (1) and (2) are essentially identical, as expected. We do not expect an exact agreement with the plane wave approximation since the input beams used in these measurements have beam waists back inside their respective lasers. However, each beam diverges slowly and the parametric interaction occurs within three Rayleigh lengths of each beam waist so that Equation (2) should be valid. Equation (1) applies to the beam waists located at the center of the crystal and should probably not be applied to the unfocused case. Equation (2) does not apply to the focused cases and Equation (1) must be used for these power calculations.

The agreement between experiment and theory is poor for all of the experiments using focused input beams. We observed approximately 20% of the calculated IR output power for the two experiments where ξ was less than the optimal value (F = 400, 250 mm) and 38% of the theoretical yield with nearly ideal focusing (F = 100 mm, ξ = 1.893). We note that the phase matching frequency of the signal laser was carefully optimized in the F= 100 mm experiments and this may partially explain the increased conversion efficiencies noted for these results.

5. THERMAL LOADING

We have several experimental indications that residual absorption in the $AgGaS_2$ crystal causes thermal loading and limits the maximum attainable IR output power. The observed turnover in P_i as P_S increases, shown in Figures 3 and 4, and the blooming of the visible beams after the crystal imply a thermally induced effect.

We have used the approximations developed by Innocenzi et al.[12] and the loss measured calorimetrically to estimate the thermal lensing effects in our experiment. A temperature gradient along the

propagation axis resulting from light absorption is expected. Such a temperature gradient might decrease the coherence length as result of the temperature dependence of the phase matching condition. Our calculations indicate that this effect is not important and may be ignored. However, the radial temperature gradient resulting from absorption causes pronounced thermal lensing of the pump and signal waves. Since dn/dT is positive for $AgGaS_2$, temperature increases create a positive thermal lens whose focal length is given by[12]

$$f_{Thermal} = \frac{\pi K_c w_p^2}{P \frac{dn}{dT}} \left(\frac{1}{1 - \exp[-\alpha L]} \right) \tag{5}$$

From Equation (5), we calculate a focal length of 6.33 mm for a thermal lens generated inside our 45 mm long $AgGaS_2$ crystal assuming $\alpha = 0.05\ cm^{-1}$, $K_c = 0.014\ W/(cm\ K)$[13], $w_p = 300\ \mu m$, $dn/dT = 1.55 \times 10^{-4}\ °C^{-1}$, and P = 2 W. The calculated $f_{Thermal}$ is much smaller than the crystal length, so the assumptions on which Equation (5) is based are invalid. However, this result suggests that overfocusing may be desirable: the strong positive focusing created by temperature gradients at the beam waist may confine the wave fronts and extend the near field region, thus increasing the effective parametric interaction length.

The phase matching is also affected by thermal effects caused by visible laser absorption. In Figure 5 the signal frequency required to maintain maximum IR output power is plotted as a function of the signal laser input power. These data were recorded simultaneously with the IR output powers presented in Figure 4. Note the nearly linear increase in ν_{signal} with P_{signal}.

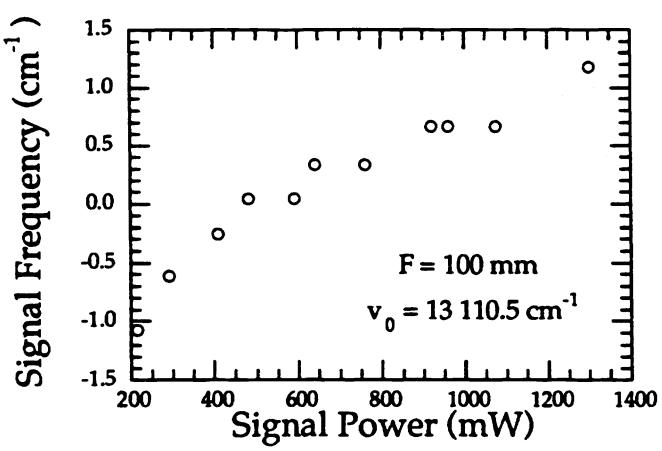

Figure 5. The signal wave frequency required to obtain maximum IR output power as a function of signal wave power input. This data was recorded simultaneously with the IR power data shown in Figure 4.

The phase matching measurements depicted in Figure 5 primarily reflect the thermal steady-state established between heat flowing into the crystal by absorption of the pump beam and heat being lost to the surroundings. The phase mismatch is related to the crystal temperature in the parametric interaction region through the temperature dependence displayed by n_p, n_s, and n_i, the refraction indices. A linear least squares evaluation of the data in Figure 5 yields $d\nu/dP = 1.8\ cm^{-1}/W$. We can estimate the power induced temperature change, dT/dP, using the value of $d\nu/dT = 0.417\ cm^{-1}/°C$ we previously determined for the temperature dependence of the phase matching conditions[14]

$$\frac{dT}{dP} = \frac{\left(\frac{d\nu}{dP}\right)}{\left(\frac{d\nu}{dT}\right)} = \frac{(1.8/0.82)\ \frac{cm^{-1}}{W}}{0.417\ \frac{cm^{-1}}{°C}} = 5.29\ \frac{°C}{W} \tag{6}$$

where we divide by 0.82 to account for Fresnel loss at the front surface of the crystal.

The radial temperature change in the crystal caused by the incident laser power is[12]

$$\frac{d(T(r) - T(r_b))}{dP} = \frac{\alpha}{4 \pi K_c} \left(\ln\left(\frac{r_b^2}{r^2}\right) + E_1\left(\frac{2r_b^2}{\omega_p^2}\right) - E_1\left(\frac{2r^2}{\omega_p^2}\right) \right) = 2.77 \frac{°C}{W} \qquad (7)$$

where α (= 0.05 cm^{-1}) is the signal power absorption coefficient, K_c(= 0.014 W/(cm K)) is the thermal conductivity coefficient, r_b is the crystal radius, ω_p(= 29 μm) is the beam waist, and $E_1(x)$ is the exponential integral. This equation assumes that the crystal is a cylinder with a 2 mm radius (our crystal has a (4 x 4) mm^2 square cross section). In our experimental arrangement the crystal is exposed to air on two sides and pressed against a thin Al housing on by teflon screws on the other two sides. We believe that the temperature at the surfaces of the crystal must be rising by about 2.5 °C/W to account for the discrepancy between the phase matching temperature rise of 5.29 °C/W of Equation (6) and the smaller estimated rise of 2.77 °C/W from Equation (7). The thermal conductivity of air is only 0.00025 W/(cm K) compared with 0.014 W/(cm K) for $AgGaS_2$.

There have been reports of similar thermal lensing behavior in the related chalcopyrite material $AgGaSe_2$.[15-17] Marquardt et al.[15] have recently demonstrated that the thermal lensing effects in a $AgGaSe_2$ OPO pumped at kilohertz repetition rates can be virtually eliminated by cooling the crystal to liquid nitrogen temperatures. We plan to explore the thermal behavior of DFG in $AgGaS_2$ at cryogenic temperatures, although this is a negative design consideration in our quest for an "ideal" IRKS source.

6. CONCLUSIONS

We have constructed a cw DFG source based on $AgGaS_2$ as the central element in a IRKS apparatus achieving output powers of 10 - 30 μW and have explored the parametric conversion efficiency as a function of focusing conditions and input powers. We observed reasonable agreement between experimental and theoretical IR yields for the limiting case of DFG with plane waves, but the optimized experimental yields for DFG from focused beams was a factor of 3 to 5 lower than the theory predicted. Thermal loading in the $AgGaS_2$ crystal was observed for all focusing conditions. Because we have more Ti:S power available (up to 2 Watts) and the IR output power begins to turn over at 800 mW, it is clear that residual absorptions in the $AgGaS_2$ crystal are limiting our ultimate IR power production.

With DFG obtained to date, we have obtained good quality IRKS spectra of the radicals HOCO and HCCN using IR powers in the 10 - 30 μW range.[1] Our attempts to measure such spectra with earlier 1-2 μW IR power levels were unsuccessful. Further increases in the IR power output will enable us to use balanced IR detectors and remove high frequency amplitude noise from our IR source for factor of ~20 increase in S/N. Increased IR conversion efficiency will be most beneficial for experiments which employ wavelengths in the 7 - 10 μm range since we expect less IR power in this range because of the ω_i^2 and μ dependences in Equation (1).

There are two improvements which we clearly must make to increase the IR output power of our $AgGaS_2$ DFG source. Firstly, the thermal loading effects in the crystal must be eliminated or significantly reduced. State of the art $AgGaS_2$ crystals currently have residual absorptions of less than 0.5% cm^{-1} compared to ~3.0% cm^{-1} for our crystal. Using more transparent $AgGaS_2$ bars should permit the use of higher pumping powers without thermal loading. With these more transparent materials, the effective pumping power can be further increased by AR coating the front surface of the crystal and loss of IR at the exit surface can be reduced by IR AR coating that surface. Without such coatings Fresnel losses at the entrance and exit surfaces would reduce the IR output power to 55% of its potential value.

7. ACKNOWLEDGMENTS

This work has been supported by the Robert A. Welch Foundation and the National Science Foundation. CEM thanks the Robert A. Welch Foundation for a post-doctoral fellowship. WCE gratefully acknowledges the Department of Defense for a pre-doctoral fellowship. U. Simon gratefully acknowledges the support of the Alexander von Humbolt Foundation by a Feodor Lynen Fellowship.

8. REFERENCES

1 C. E. Miller, U. Simon, W. C. Eckhoff, R. F. Curl, and F. K. Tittel, "Infrared Kinetic Spectroscopy of Free Radicals Using Difference Frequency Generation," in *Laser Spectroscopy: XIth International Conference*, AIP Conference Proceedings No. 290, L. Bloomfield, T. Gallagher, and D. Larson, eds., New York, 1993, pp. 122-127.

2 K. G. Unfried and R. F. Curl, "Infrared Flash Kinetic Spectroscopy of ν_2 of Ketenyl Radical," *J. Mol. Spectrosc.*, Vol. 150, pp. 86-98, 1991.

3 R. F. Curl, K. L. Murray, M. Petri, M. L. Richnow, and F. K. Tittel, "Infrared Spectroscopy of Jet-cooled Transient Molecules," *Chem. Phys. Lett.*, Vol. 161, pp. 98-102, 1989.

4 J. W. Stevens, W.-B. Yan, M. L. Richnow, H. Solka, and R. F. Curl, "Infrared Kinetic Spectroscopy of C_2H and C_2D," *J. Mol. Struct.*, Vol. 190, pp. 41-60, 1988.

5 G. D. Boyd and D. A. Kleinman, "Parametric Interaction of Focused Gaussian Light Beams," *J. Appl. Phys.*, Vol. 39, pp. 3597-3639, 1968.

6 T.-B.-Chu and M. Broyer, "Intracavity cw Difference Frequency Generation by Mixing Three Photons and Using Gaussian Beams," *J. de Physique (Paris)*, Vol. 46, pp. 523-533.

7 P. Canerelli, Z. Benko, R. F. Curl, and F. K. Tittel, "Continuous-wave Infrared Laser Spectrometer Based on Difference Frequency Generation in $AgGaS_2$ for High Resolution Spectroscopy," *J. Opt. Soc. Am. B*, Vol. 9, pp. 197-202, 1992.

8 G. C. Catella, private communication.

9 G.D. Boyd, H. Kasper, and J. H. McFee, "Linear and Nonlinear Optical Properties of $AgGaS_2$, $CuGaS_2$, $CuInS_2$, and Theory of the Wedge Technique for the Measurement of Nonlinear Coefficients," *IEEE J. Quantum Electron.*, Vol QE-7, pp. 563 - 573, 1971.

10 G. C. Bhar and R. C. Smith, "Silver Thiogallate ($AgGaS_2$) - Part II: Linear Optical Properties," *IEEE J. Quantum Electron.*, Vol QE-10, pp. 546-550, 1974.

11 T. F. Johnson and M. W. Sasnett, "The Effect of Pump Laser Mode Quality on the Mode Quality of the CW Dye Laser," *Laser Energy Distribution Profiles: Measurement and Applications*, SPIE Proceedings, Vol. 1834, 1993.

12 M. E. Innocenzi, H. T. Yura, C. L. Fincher, and R. A. Fields, "Thermal Modeling of Continuous-wave End-pumped Solid-state Lasers," *Appl. Phys. Lett.*, Vol. 56, pp. 1831-1833, 1990.

13 J. D. Beasley, "Thermal Conductivities of Some Novel Nonlinear Optical Materials," *Appl. Opt.* (to be published).

14 P. Canerelli, Z. Benko, A. H. Hielscher, R. F. Curl, and F. K. Tittel, "Measurement of Nonlinear Coefficient and Phase Matching Characteristics of $AgGaS_2$," *IEEE J. Quantum Electron.*, Vol. 28, pp. 52-55, 1992.

15 C.L. Marquardt, D. G. Cooper, P.A. Budni, M. G. Knights, K. L. Schepler, R. DeDomenico, and G. C. Catella, "Thermal Lensing in $AgGaSe_2$ OPO Crystals," *Appl. Opt.* (to be published).

16 P. A. Budni, M. G. Knights, E. P. Chicklis, and K. L. Schepler, "Kilohertz pumped Optical Parametric Oscillator Pumped at 2 μm," *Opt. Lett.*, Vol. 18, pp. 1068-1070, 1993.

17 G. C. Catella, L. R. Shiozawa, J. R. Hietanen, R. C. Eckardt, R. K. Route, R. S. Feigelson, D. G. Cooper, and C. L. Marquardt, "Mid-IR Absorption in $AgGaSe_2$ Optical Parametric Oscillator Crystals," *Appl. Opt.*, Vol. 32, pp. 3948-3950, 1993.